Journal of the Optical Society of America A
OPTICS, IMAGE SCIENCE, AND VISION

Point-by-point near-field optical energy deposition around plasmonic nanospheres in absorbing media

R. K. Harrison and Adela Ben-Yakar*

Mechanical Engineering, University of Texas at Austin, 1 University Station C2200, Austin, Texas 87112, USA
**Corresponding author: ben-yakar@mail.utexas.edu*

Received 6 May 2015; revised 19 June 2015; accepted 20 June 2015; posted 22 June 2015 (Doc. ID 240275); published 21 July 2015

Here we investigate the effects of absorbing media on plasmon-enhanced near-field optical energy deposition. We find that increasing absorption by the medium results in increased particle scattering at the expense of particle absorption, and that much of this increased particle scattering is absorbed by the medium close to the particle surface. We present an analytical method for evaluating the spatial distribution of near-field enhanced absorption surrounding plasmonic metal nanospheres in absorbing media using a new point-by-point method. We propose criteria to define relevant near-field boundaries and calculate the properties of the local absorption enhancement, which redistributes absorption to the near-field and decays asymptotically as a function of the distance from the particle to background levels. Using this method, we performed a large-scale parametric study to understand the effect of particle size and wavelength on the near-field absorption for gold nanoparticles in aqueous media and silicon, and identified conditions that are relevant to enhanced local infrared absorption in silicon. The presented approach provides insight into the local energy transfer around plasmonic nanoparticles for predicting near-field effects for advanced concepts in optical sensing, thin-film solar cells, nonlinear imaging, and photochemical applications.

OCIS codes: (250.5403) Plasmonics; (290.4020) Mie theory; (160.4236) Nanomaterials; (290.5850) Scattering, particles; (230.2090) Electro-optical devices; (170.4520) Optical confinement and manipulation.

http://dx.doi.org/10.1364/JOSAA.32.001523

1. INTRODUCTION

The extraordinary optical response of plasmonic metal nanoparticles has become a topic of great scientific interest. Recent advances in the scientific understanding of plasmonics has led to the application of plasmonic metal nanoparticles as biomedical contrast agents for multiphoton imaging [1], for the targeted photothermal destruction of tissue [2], photodynamic therapy [3], plasmonic laser nanoablation [4,5], optical data storage [6], solar cell absorption enhancement [7], photocatalysis [8], and multiphoton polymerization [9], among many others [10].

Various applications of plasmonic particles require a thorough understanding of not only the interaction of light with nanoparticles, but also how the energy is transferred from the particle to the surrounding region, especially in the close vicinity known as the near-field. Energy transfer can be through processes such as the redirection of optical energy flow through scattering, the thermal transfer of heat from the particle to its surrounding, and the electrons and ions ejected from the particle. The scattered light from the particle can be absorbed by the surrounding media through linear or nonlinear processes depending on the intensity of the incoming light. Several previous studies have examined the transfer of thermal energy from a nanoparticle to the surrounding region [11,12]. Others showed that near-threshold ablation of plasmonic nanoparticles preferentially occurs near the poles of the particle, providing a link between experimental observations of ablation and calculated near-field properties [13]. Our group and others have used ultrafast lasers to study plasmonic particle-mediated ablation patterns to create near-field enhancement "snapshots" [4,5,14,15]. A primary goal in these studies was not only to understand the plasmonic response of nanoparticle systems, but also to determine the mechanisms by which optical energy "focused" on the particle near-field is transferred to their surroundings. By understanding optical energy transfer, especially in absorbing media, nanoparticles and techniques can be designed more effectively for advanced plasmonic applications in the medical, sensor, and energy sectors.

Plasmonic particles embedded in absorbing media are an especially interesting topic, as the boundary conditions are affected significantly, even by a weak imaginary component

of the refractive index of the medium. This topic has drawn limited research, but a deeper understanding of the implications of the effects of an absorbing medium on the plasmonic response could impact a wide range of applications, including low-energy photon upconversion, enhanced LED emission, photosensitization to promote the absorption of dyes in photodynamic therapy, fluorophores emission enhancement for molecular detection, enhancement of chemical processes in photocatalysis, and the localization and enhancement of absorbed light in plasmonic photopolymerization. Furthermore, plasmon-enhanced local absorption could improve photoconversion efficiency in semiconductor detectors and photovoltaics, especially for poorly absorbed near-bandgap long wavelength photons. This technique could be employed potentially by using plasma deposition of silicon over nanoparticles, with solution deposited semiconductors or organic photovoltaics, or using degenerately doped "metal-like" semiconductor regions using standard photolithography techniques to fabricate plasmonic elements directly within a semiconductor medium.

Optimizing plasmonic particles to achieve maximum benefits for each of these disparate applications should be performed ideally using simulations, but existing tools are inadequate for this purpose. Time-consuming numerical computational methods are available to calculate near-field absorption around plasmonic particles, but existing iterative numerical methods for determining the energy deposition at arbitrary locations surrounding plasmonic nanoparticles, such as finite difference time domain (FDTD), can be computationally prohibitive for performing large-scale parametric optimizations. Thus, it would be of significant interest to develop a more rapidly computed analytical solution method to explore absorption surrounding particles of various materials and matrices over a broad spectrum of wavelengths and particle sizes.

For the special case of spherical particles in dielectric media, analytical solutions in the form of the Mie theory can be used to calculate the electromagnetic fields in and around a particle. An extended Mie theory was developed to evaluate the effect of absorbing media on particle optical interaction efficiencies. However, there is also interest in understanding the near-field effects on local absorption. Near-field enhancement is especially important in the presence of absorbing materials, where enhanced fields can directly lead to increased optical deposition of energy.

One method for evaluating absorption around a plasmonic nanoparticle embedded in an absorbing medium employs an extended Mie theory through the use of concentric shells to determine the total absorption at various ranges. Several noteworthy studies have used this method in conjunction with spherical control volumes concentric on a nanoparticle to determine the total linear optical absorption within a shell region surrounding a plasmonic nanosphere [16,17]. This method, however, cannot provide information on the spatial distribution of the enhanced absorption. Since the region of near-field enhancement is not spherical, a concentric shell approach will include both enhanced and unenhanced regions in the particle near-field, resulting in a blurring of the actual enhancement volume. This averaged enhancement value will lead to inaccurate estimates in the presence of highly localized or nonlinear effects, for example.

An alternate approach for determining the optical energy absorption in an absorbing medium at arbitrary locations can be found by simplifying the Poynting theorem to a function of the $|\boldsymbol{E}|^2$ field only. Notably, Baffou *et al.* studied local heat generation in plasmonic nanoparticles using this method [18]. However, the presence of interacting fields complicates the interpretation of this calculation in the region outside a plasmonic nanoparticle. In the near-field region, the electromagnetic fields generated by the resonant nanoparticle plasmons substantially affect the flow of the incident light, creating an optical "vortex" drawing in light from an area much larger than the particle itself. Previously, we have shown that the local ratio of the electric-to-magnetic field in this region deviates significantly from its characteristic value in the near-field of a plasmonic nanoparticle [19]. Here, we are interested in investigating the effect of this disruption on near-field absorption. Furthermore, an expanded solution to the problem of enhanced absorption around a spherical object can reveal the relative contributions of different sources to near-field enhancement and absorption.

To address questions about near-field energy transfer and to provide a simpler method for performing large-scale parametric optimizations, we analytically derived a new point-by-point method to calculate the local near-field absorption in the medium outside a plasmonic nanosphere.

One important application of a point-by-point approach is in estimating the plasmonic enhancement of thin film solar photovoltaics or optical sensors [20]. In this case, the charge collection efficiency can be limited by the thickness, creating a tradeoff with the corresponding optical absorption. One proposed approach involves the incorporation of the plasmonic nanoparticle directly within an absorber material [7]. In this example, the intensity and location of absorption can influence significantly the charge collection efficiency in thin film photoelectric devices. Therefore, understanding the spatial dependence of absorption around integrated nanoparticles could enable more effective plasmonic designs through the optimization of the nanoparticle position and spacing. This method could also be useful for designing very sensitive thin film wavelength dependent sensors for imaging applications.

For many applications, the spatial extent and concentration of deposited light can be more important than the total optical interaction that typically is calculated from far-field extinction. Specifically, intensity-dependent effects such as saturation, photobleaching, and multiphoton absorption require the calculation of near-field optical absorption on a point-by-point basis. To date, there has been relatively little work in comparing the local or net near-field enhancement with increased absorption. Notable correlations have been observed, including enhanced multiphoton-polymerization in the near-field of metallic features [9], but further examinations of near-field optical absorption are necessary for a full understanding of these effects.

Plasmonic metal nanoparticles have become ubiquitous in studies ranging from photonics to biomedical engineering, but many aspects of near-field enhancement remain unexplored, especially in the presence of an absorbing medium.

For example, what portion of the scattered light contributes to the near-field absorption and how does this absorption depend on the particle size and the absorption coefficient of the medium? What are the size and shape of the near-field enhanced absorption region and what delimits the near-field boundary? These questions rarely are posed, but can provide great insight into plasmonic enhancement mechanisms when addressed [21]. It can be difficult to design experiments to probe enhancement effects because of the nanometer scale and ultrafast time scales of plasmonic near-field effects. Experimental results often can lead to ambiguity where several different physical mechanisms could cause observed experimental phenomena [22].

To address these issues, we have developed a mathematical framework for calculating the point-by-point enhanced deposition of energy in the near-field of plasmonic nanospheres embedded in absorbing media. Using this method, we analyze important trends and present results determining the optimal sizes for near-field enhanced absorption for gold nanospheres (AuNP) embedded in aqueous media and silicon as an example of the utility of this technique.

2. THEORY AND METHODS

A. Optical Interaction Efficiencies of Nanoparticles in an Absorbing Medium

The conservation of energy for electromagnetic fields is given by the Poynting theorem [23]:

$$\oint_A \boldsymbol{S}\cdot\hat{\boldsymbol{n}}\mathrm{d}A = -\frac{1}{2}\int_V \boldsymbol{J}^*\cdot\boldsymbol{E}\mathrm{d}V - \frac{1}{2}\int_V\left(\boldsymbol{E}\cdot\frac{d\boldsymbol{D}}{dt}+\boldsymbol{H}\cdot\frac{d\boldsymbol{B}}{dt}\right)\mathrm{d}V. \quad (1)$$

The Poynting theorem states that the flow of energy across a control boundary (left-hand side) is equivalent to the amount of energy consumed within the control volume as a result of the electromagnetic interactions (right-hand side). Here, we are interested primarily in the time-averaged properties of harmonic electromagnetic fields. The flow of energy across the boundary is given by the normal component of the complex Poynting vector, $\boldsymbol{S}$, integrated across the control volume surface. The first and second terms on the right side refer to the conduction heating and energy stored in the electromagnetic fields within the volume, respectively. The complex Poynting vector describes the magnitude and direction of electromagnetic flow at a specific location and is given by the cross product of the electric and magnetic fields:

$$\boldsymbol{S} = \frac{1}{2}(\boldsymbol{E}\times\boldsymbol{H}^*) = \frac{1}{2}(\boldsymbol{E}_{\mathrm{inc}}+\boldsymbol{E}_{\mathrm{sca}})\times(\boldsymbol{H}^*_{\mathrm{inc}}+\boldsymbol{H}^*_{\mathrm{sca}}) \quad (2)$$

Here asterisks indicate the complex conjugate of the value, and bold typeface indicates vectors. The optical electric field, $\boldsymbol{E}$, and magnetic field, $\boldsymbol{B}$, present around any arbitrary scatterer consist of a superposition of the electromagnetic fields between the incident (inc) and scattered (sca) light present at each point in space. Thus, the total complex Poynting vector can be described in terms of the scattered fields, $\boldsymbol{S}_{\mathrm{sca}}$, the incident fields, $\boldsymbol{S}_{\mathrm{inc}}$, and the interaction between these fields, known as the extinction term, $\boldsymbol{S}_{\mathrm{ext}}$:

$$\begin{aligned}\boldsymbol{S} &= \boldsymbol{S}_{\mathrm{sca}}+\boldsymbol{S}_{\mathrm{inc}}+\boldsymbol{S}_{\mathrm{ext}}\\ \boldsymbol{S}_{\mathrm{sca}} &= \frac{1}{2}(\boldsymbol{E}_{\mathrm{sca}}\times\boldsymbol{H}^*_{\mathrm{sca}})\\ \boldsymbol{S}_{\mathrm{inc}} &= \frac{1}{2}(\boldsymbol{E}_{\mathrm{inc}}\times\boldsymbol{H}^*_{\mathrm{inc}})\\ \boldsymbol{S}_{\mathrm{ext}} &= \frac{1}{2}(\boldsymbol{E}_{\mathrm{inc}}\times\boldsymbol{H}^*_{\mathrm{sca}}+\boldsymbol{E}_{\mathrm{sca}}\times\boldsymbol{H}^*_{\mathrm{inc}}).\end{aligned} \quad (3)$$

The energy flow across a nanoparticle (NP) surface can, in general, be calculated by the integration of the scalar product of the Poynting vector with a unit vector surface normal $\hat{n}$ over the particle surface. The total energy flow across the particle boundary is absorbed by the nanoparticle and remains as heat. It is common to define the nondimensional absorption efficiency of the nanoparticle, Q, through a normalization by the amount of optical energy incident on the area "shadowed" by the particle, $I_z A_{\mathrm{CS}}$, where I_z is the incident intensity at the depth of the center of the sphere (i.e., the intensity reaching the plane of the particle center) and A_{CS} is the geometrical cross section of the particle:

$$Q_{\mathrm{abs,NP}} = \frac{-1}{I_z A_{\mathrm{CS}}}\oint_{\mathrm{NP}} \boldsymbol{S}\cdot\hat{\boldsymbol{n}}\mathrm{d}A. \quad (4)$$

Each component of the Poynting vector can be integrated similarly over the area of the particle surface to determine the constituent optical interaction efficiencies:

$$\begin{aligned}Q_{\mathrm{ext,NP}} &= \frac{-1}{I_z A_{\mathrm{CS}}}\oint_{\mathrm{NP}} \boldsymbol{S}_{\mathrm{ext}}\cdot\hat{\boldsymbol{n}}\mathrm{d}A\\ Q_{\mathrm{sca,NP}} &= \frac{1}{I_z A_{\mathrm{CS}}}\oint_{\mathrm{NP}} \boldsymbol{S}_{\mathrm{sca}}\cdot\hat{\boldsymbol{n}}\mathrm{d}A\\ Q_{\mathrm{inc,NP}} &= \frac{-1}{I_z A_{\mathrm{CS}}}\oint_{\mathrm{NP}} \boldsymbol{S}_{\mathrm{inc}}\cdot\hat{\boldsymbol{n}}\mathrm{d}A.\end{aligned} \quad (5)$$

These efficiencies can be much larger than 1 in the case of plasmonic nanoparticles on resonance, indicating that the particle draws in light from an area significantly larger than the particle itself. This effect occurs because of the strong resonant interaction between the collective oscillations of electrons in the particle and the incident light. The sum of these efficiency terms provides the fundamental optical interaction expression in terms of the extinction efficiency of the nanoparticle, $Q_{\mathrm{ext,NP}}$:

$$Q_{\mathrm{ext,NP}} = Q_{\mathrm{sca,NP}} + Q_{\mathrm{abs,NP}} - Q_{\mathrm{inc,NP}}. \quad (6)$$

The $Q_{\mathrm{abs,NP}}$ term represents the contribution of absorption occurring in the particle itself and the $Q_{\mathrm{inc,NP}}$ term represents the contribution of absorption that would have been occurring in the displaced medium material corresponding to the volume of the nanoparticle, namely the amount of energy absorbed by the medium in the absence of the particle. This incident efficiency term obviously vanishes for nonabsorbing media and, thus, is not included in the standard expression of the optical interaction theorem. The general term for $Q_{\mathrm{ext,NP}}$, however, must include the effect of $Q_{\mathrm{inc,NP}}$. Mie theory provides analytical solutions to optical efficiency terms for a nonabsorbing medium ($Q_{\mathrm{inc,NP}} = 0$) [24,25], when real arguments are provided for the refractive index of the medium. For an absorbing medium, however, we need to account for a complex

refractive index in the medium [26]. To calculate the optical efficiencies for spherical particles in an absorbing medium ($Q_{\mathrm{inc,NP}} > 0$), we therefore used an extended Mie theory, where our derivations are equivalent to expressions presented in the literature [27,28]. As expected, these equations simplify to the standard Mie theory expressions when real arguments are provided for the refractive index of the medium.

B. Point-by-Point Local Energy Deposition around a Nanosphere

To calculate the local energy deposition at each point in the absorbing media around nanospheres, we propose to replace the surface integral in Eq. (1) with a point-by-point volume integral according to the divergence theorem:

$$\oint_A \boldsymbol{S}\cdot\hat{\boldsymbol{n}}\mathrm{d}A = \int_V \nabla\cdot\boldsymbol{S}\mathrm{d}V. \tag{7}$$

The divergence of the complex Poynting vector represents the local energy consumed at each point in space around the particle, and can be calculated by using the formula for $\boldsymbol{S}$ from Eq. (2):

$$\nabla\cdot\boldsymbol{S} = \nabla\cdot\frac{1}{2}(\boldsymbol{E}\times\boldsymbol{H}^*) = \frac{1}{2}[\boldsymbol{H}^*\cdot(\nabla\times\boldsymbol{E}) - \boldsymbol{E}\cdot(\nabla\times\boldsymbol{H}^*)]. \tag{8}$$

To calculate the electric and magnetic fields in an absorbing medium, we use the expansion of fields in spherical vector harmonics similarly to standard Mie theory [25], but in this case, the wave number k, scattering coefficients (a_n and b_n), and Riccati–Bessel functions (ψ_n and ξ_n) are all complex. The energy absorbed at each point in space can be obtained by discretizing the near-field region and directly solving for the energy absorbed in each small volume unit.

Starting from the field equations presented in Mie theory [25], we first determine the curl of the total electric fields resulting from the interaction of a plane wave with spherical particle from both the incident and scattered waves:

$$(\nabla\times\boldsymbol{E})_r = \frac{\sin\phi}{r\sin\theta kr}\sum_{n=1}^{\infty}E_n((\pi_n-\tau_n\cos\theta-\sin\theta\tau_n')(\psi_n-b_n\xi_n) + i(\tau_n-\pi_n\cos\theta-\pi_n'\sin\theta)(-\psi_n'+a_n\xi_n')) \tag{9}$$

$$(\nabla\times\boldsymbol{E})_\theta = \frac{\sin\phi}{r}\sum_{n=1}^{\infty}E_n\left(i\pi_n(-\psi_n''+a_n\xi_n'')+\tau_n(\psi_n'-b_n\xi_n') + i\pi_n n(n+1)\left(\frac{\psi_n}{(kr)^2}-a_n\frac{\xi_n}{(kr)^2}\right)\right) \tag{10}$$

$$(\nabla\times\boldsymbol{E})_\phi = \frac{\cos\phi}{r}\sum_{n=1}^{\infty}E_n\left(\pi_n(\psi_n'-b_n\xi_n')+i\tau_n(-\psi_n''+a_n\xi_n'') + in(n+1)(\cos\theta\pi_n+\sin\theta\pi_n')\left(\frac{\psi_n}{(kr)^2}-a_n\frac{\xi_n}{(kr)^2}\right)\right). \tag{11}$$

Likewise, the vector components of the curl of the magnetic field are given as

$$(\nabla\times\boldsymbol{H})_r = -\frac{\cos\phi}{r\sin\theta kr}\frac{k}{\omega\mu}\sum_{n=1}^{\infty}E_n((\pi_n-\cos\theta\tau_n-\sin\theta\tau_n')\times(\psi_n-a_n\xi_n)+i(\tau_n-\cos\theta\pi_n-\sin\theta\pi_n')(-\psi_n'+b_n\xi_n')) \tag{12}$$

$$(\nabla\times\boldsymbol{H})_\theta = \frac{-\cos\phi}{r}\frac{k}{\omega\mu}\sum_{n=1}^{\infty}E_n\left(\tau_n(\psi_n'-a_n\xi_n')+i\pi_n(-\psi_n''+b_n\xi_n'') + in(n+1)\pi_n\left(\frac{\psi_n}{(kr)^2}-b_n\frac{\xi_n}{(kr)^2}\right)\right) \tag{13}$$

$$(\nabla\times\boldsymbol{H})_\phi = \frac{-\sin\phi}{r}\frac{k}{\omega\mu}\sum_{n=1}^{\infty}E_n\left(\pi_n(-\psi_n'+a_n\xi_n')+i\tau_n(\psi_n''-b_n\xi_n'') + in(n+1)(\cos\theta\pi_n+\sin\theta\pi_n')\times\left(-\frac{\psi_n}{(kr)^2}+b_n\frac{\xi_n}{(kr)^2}\right)\right). \tag{14}$$

The variable r in Eqs. (9)–(14) is the radius and k is the wave number of light in the medium surrounding the particle ($k = 2\pi m/\lambda$). The azimuthal angle is given by ϕ and the polar angle is denoted θ. The wavelength of light in a vacuum is given by λ, and the real and imaginary parts of the refractive index of the surrounding medium are $m = \eta + i\kappa_M$, where subscript M indicates medium. The rotational frequency of the light is given by ω, and the magnetic permeability is μ. To calculate the curl of the fields, we need to find the values of the second derivatives of the Riccati–Bessel functions, ψ_n'' and ξ_n'' for each order n of the expansion. We derive these terms by taking the derivative of the recursion relationships:

$$\psi_n'' = \psi_{n-1}' - \frac{n\psi_n'}{kr} + \frac{n\psi_n}{(kr)^2} \tag{15}$$

$$\chi_n'' = \chi_{n-1}' - \frac{n\chi_n'}{kr} + \frac{n\chi_n}{(kr)^2} \tag{16}$$

$$\xi_n'' = \psi_n'' - i\chi_n''. \tag{17}$$

The derivatives of the angular π_n and τ_n terms also must be calculated for each order of expansion from the suitable recursion relationships given in Eqs. (18) and (19). The initial conditions of the angular functions for the first few orders are shown in Eqs. (20) and (21). Subsequent terms can be determined using upward recursion relationships for an increasing order n:

$$\pi_{n+1}' = \frac{2n-1}{n-1}(\cos\theta\pi_n' - \sin\theta\pi_n) - \frac{n}{n-1}\pi_{n-1}' \tag{18}$$

$$\tau_{n+1}' = n(\cos\theta\pi_{n+1}' - \sin\theta\pi_{n+1}) - (n+1)\pi_n' \tag{19}$$

$$\pi_0' = 0, \pi_1' = 0, \pi_2' = -3\sin\theta \tag{20}$$

$$\tau_0' = 0, \tau_1' = \sin\theta, \tau_2' = -12\sin\theta\cos\theta. \tag{21}$$

With all the components determined in Eqs. (9)–(21), the total absorption at a given point $\nabla\cdot\boldsymbol{S}$ outside a spherical particle can be solved by using Eq. (8). A local normal energy flow calculation across all bounding surfaces of a discrete volume

element, similar to using the left-hand side of Eq. (7), could also be used to find local energy deposition.

C. Near-Field Absorption Efficiency Terms in the Medium around a Nanosphere

Outside the particle, three different sources contribute to near-field absorption in the medium: the incident field ($\nabla \cdot \boldsymbol{S}_{\text{inc}}$), scattered field ($\nabla \cdot \boldsymbol{S}_{\text{sca}}$), and an interacting field term ($\nabla \cdot \boldsymbol{S}_{\text{ext}}$):

$$\nabla \cdot \boldsymbol{S} = \nabla \cdot \boldsymbol{S}_{\text{sca}} + \nabla \cdot \boldsymbol{S}_{\text{ext}} + \nabla \cdot \boldsymbol{S}_{\text{inc}}. \tag{22}$$

The absorption in the medium because of the incident field ($\nabla \cdot \boldsymbol{S}_{\text{inc}}$) corresponds to the amount of energy absorbed at a given position because of the incident field only (i.e., the absence of a particle). The scattered and incident light contributions to their respective near-field absorption efficiency terms are always positive by definition, as they represent the absorption of light in the medium. The interaction term ($\nabla \cdot \boldsymbol{S}_{\text{ext}}$), which represents the effect of the interaction between the incoming and scattered light on the local absorption, can be positive or negative. The sign and magnitude will depend on whether the wave interference between the incident and scattered waves is constructive or destructive at that location. The "extra" light absorbed in the near-field region is the sum of the scattered ($\nabla \cdot \boldsymbol{S}_{\text{sca}}$) and interaction ($\nabla \cdot \boldsymbol{S}_{\text{ext}}$) field contributions to absorption in the medium outside the particle.

Using these identified terms, we then can define the absorption enhancement factor F_{AE}, which is given by the quotient of the total local absorption in the medium and the energy absorbed from the incident light only:

$$F_{AE} = \frac{\nabla \cdot \boldsymbol{S}}{\nabla \cdot \boldsymbol{S}_{\text{inc}}}. \tag{23}$$

This parameter is equivalent to dividing the plasmonic enhanced absorption by what would be absorbed over the same volume in the absence of the particle. This term can be calculated for discrete volume elements, or averaged over the whole near-field region, which we denote $\bar{F}_{AE}$.

The proposed point-by-point integration method now provides the ability to calculate the enhancement of near-field absorption contributed by each component by integrating each term over the near-field volume, V_{NF}, occupying the region outside the sphere in the absorbing medium. We can then easily define near-field absorption efficiency terms for each component similar to the standard optical interaction efficiencies of the particle [Eq. (5)] by normalizing each of these terms with the optical power of the incident beam at the midpoint of the particle, $I_z A_{\text{CS}}$:

$$\begin{aligned} Q_{\text{abs,NF}} &= \frac{-1}{I_z A_{\text{CS}}} \oint_{V_{\text{NF}}} \nabla \cdot \boldsymbol{S} \mathrm{d}V \\ Q_{\text{ext,NF}} &= \frac{-1}{I_z A_{\text{CS}}} \oint_{V_{\text{NF}}} \nabla \cdot \boldsymbol{S}_{\text{ext}} \mathrm{d}V \\ Q_{\text{sca,NF}} &= \frac{-1}{I_z A_{\text{CS}}} \oint_{V_{\text{NF}}} \nabla \cdot \boldsymbol{S}_{\text{sca}} \mathrm{d}V \\ Q_{\text{inc,NF}} &= \frac{-1}{I_z A_{\text{CS}}} \oint_{V_{\text{NF}}} \nabla \cdot \boldsymbol{S}_{\text{inc}} \mathrm{d}V. \end{aligned} \tag{24}$$

Using the definition given in Eq. (22), we can then describe the total near-field absorption efficiency as

$$Q_{\text{abs,NF}} = Q_{\text{sca,NF}} + Q_{\text{ext,NF}} + Q_{\text{inc,NF}}. \tag{25}$$

The total near-field efficiency term includes both the regular absorption in the absence of the particle ($Q_{\text{inc,NF}}$) and the additional absorption induced by the particle which we define as a new term called the additional near-field absorption efficiency:

$$Q_{\text{add,NF}} = Q_{\text{sca,NF}} + Q_{\text{ext,NF}}. \tag{26}$$

3. COMPUTATIONAL METHOD AND VALIDATION

A. Computational Methods

For all calculations, we developed custom-written codes in Matlab based on an extended Mie theory to calculate the electromagnetic fields (electric $\boldsymbol{E}$, magnetic $\boldsymbol{B}$, and Poynting vector $\boldsymbol{S}$) at any point in the space inside, at the surface, or outside the spherical particles in the spherical or Cartesian coordinates. All fields are presented relative to the incident intensity of the nonenhanced fields of the incident light at that location in space.

To calculate the energy absorbed at each point in space outside the particle, we discretized the near-field region and directly solved for the energy absorbed in each small discrete volume element, ΔV_{mno}, starting from the surface of the nanoparticle. For each radial step m, the absorption is determined for each polar (θ_n) and azimuthal angle (ϕ_o) pair. The size of a volume element, ΔV_{mno}, depends on the position in spherical coordinates according to

$$\begin{aligned} \Delta V_{mno} = \frac{1}{3}\Delta\phi \left[\cos\left(\theta_n - \frac{1}{2}\Delta\theta\right) + \cos\left(\theta_n + \frac{1}{2}\Delta\theta\right)\right] \\ \times \left\{\left(r_m + \frac{1}{2}\Delta r\right)^3 - \left(r_m - \frac{1}{2}\Delta r\right)^3\right\}, \end{aligned} \tag{27}$$

where m, n, and o are the indices identifying the individual volume elements, r_m is the radius of the center of the volume element from the center of the nanoparticle, and $\Delta\theta$, $\Delta\phi$, and Δr are the step sizes. We performed our calculations by incrementing the radius until no angle pairs at a given radius spherical shell satisfied the near-field criterion that will be discussed next. To evaluate the total near-field energy absorption, for example, we then summed over all discrete volume elements (m, n, and o).

The refractive indices for water across the visible spectrum are calculated using a Sellmeier-type equation that fits experimental observations of the optical response [29]. The refractive indices of gold [30] and silicon [31] at each wavelength are interpolated from tabulated experimental data. We assume that the beam is large in comparison with the particle, and that the plane wave approximation is valid. In our chosen geometry, the wave travels in the positive z direction, which implies that there is constant intensity for z planes, and that the light is polarized linearly along the x-axis. Though we assume linear polarization, the spherical symmetry of the examined particles implies that these results are also valid for unpolarized incident light conditions.

B. Validation

We verified our calculations through various validation efforts and benchmark calculations for a gold sphere in a linearly absorbing water-like medium. We first compared our analytical expressions for the optical response of a sphere embedded in an absorbing medium to published results and found that they matched well with reported values and trends in Refs. [27,28]. The equations for the scattering coefficients were verified further for internal consistency using direct matrix inversion of the linear equations developed using the boundary conditions for the spherical geometry. These tests validated that our analytical series expansions could be used as a benchmark for further studies.

We then checked the calculation of the electric and magnetic fields by determining the incident and scattered fields on a spherical shell control volume surrounding the particle. By numerically integrating the radial components of the various Poynting vector constituents across the area of a spherical shell, we could check the calculated efficiencies against the analytical series expansion calculations. The numerical values should be checked at the sphere surface in absorbing media to examine the optical response at the particle. These tests yielded very satisfactory agreement with the analytical expressions, where the relative error decreased exponentially to less than 2.2×10^{-6} for $Q_{sca,NP}$, $Q_{abs,NP}$, and $Q_{ext,NP}$ at an angular step size of 0.5° at the sphere surface for a 50 nm gold sphere on resonance in a water-like medium with an imaginary refractive index of $\kappa_M = 0.2$. The internal fields within the sphere could also be checked against the absorption efficiency by setting the shell radius vanishingly close to the sphere surface (arbitrarily chosen as 10^{-9} nm, in this case), resulting in similar accuracy. The limiting behavior also can be used to verify that calculations match expected trends. As the radius became large, the absorption within a spherical control volume surrounding a particle approached the absorption of the medium, as expected. Additionally, optical fields and interaction efficiencies calculated using extended Mie theory expressions were found to yield identical results for nonabsorbing media ($\kappa_M = 0$) and in the limit of the negligible absorption ($\kappa_M = 10^{-6}$) as standard Mie theory.

Subsequently, we studied the accuracy of our point-by-point calculations as a method for calculating the absorption in the medium. We numerically integrated the divergence of the Poynting vector over the volume of the particle to find directly the total absorption of energy by the particle. As shown in Eq. (7), this calculation is equivalent (albeit more computationally intensive) to the surface integral expression for the absorption efficiency. These calculations yielded excellent agreement with our analytical expressions, reaching a relative error of 1.2×10^{-7} under the same conditions as before. We set the spatial discretization such that the fields could be approximated as constant over the small volume elements. Specifically, we set the number of radial steps equal to the particle radius divided by the number of angular steps, but the calculations were relatively insensitive to radial step size.

Finally, we compared our point-by-point volumetric calculations against spherical shell control volume calculations at various radii outside the particle in a linearly absorbing medium for multiple metals, wavelengths, shell radii, and imaginary refractive indices of the medium. Additionally, derivations for absorption within the shell of a coated sphere were used to verify the energy absorption in a spherical shell region outside the particle if the shell material was set equal to the environment. Similar agreement ($\sim 10^{-6}$ relative error) was found between the coated sphere solutions, the control volume shell solutions, and point-by-point volume divergence values, validating our presented calculation method.

4. RESULTS AND DISCUSSION

Here, we present examples for optical absorption enhancement in a generic absorbing medium and for silicon to demonstrate the type of calculations that can be obtained only by using a three-dimensional, point-by-point method. First, we used this method to calculate the optical interaction efficiencies for gold particles in absorbing media to display the effect of absorption in the medium on the plasmonic response. We then defined a criterion to better distinguish the boundaries of enhanced near-field region. Using this criterion and the proposed three-dimensional point-by-point method, we could evaluate the properties and parameters of the near-field enhancement, and their variation, as we extend from the near- to far-field region. Finally, we applied this technique to determine the enhanced absorption efficiency of the medium in the particle near-field as a function of the particle size, wavelength, and absorbing medium.

A. Optical Interaction Efficiencies of AuNP in Absorbing Media

To identify the effects of absorption within the medium on the plasmonic properties of metal nanospheres, we first examined their plasmonic response for different absorbing media using the extended Mie theory. Dielectric particles in absorbing media have been studied in some detail (e.g., [26–28]), but fewer studies have addressed theoretically the metallic particles in absorbing media [16,17,32,33]. Specifically, we performed our calculations for gold spheres (AuNP) embedded in two relevant media: (1) in water with a hypothetical absorbing dye at various concentrations, and (2) in silicon. By adding an imaginary refractive index ($\kappa_M = 0$, 0.05, 0.1 and 0.2) component to water, we could simulate the properties of India ink, carbon black pigment, or the black dye used in dye-sensitized solar cells over the visible to NIR spectrum ($\lambda = 400$ – 1000 nm). The wavelength range is selected to cover the region of interest for plasmonic particles in aqueous media, optical sensors, and solar cells. Note that an imaginary component of $\kappa_M = 0.2$ represents strong absorption corresponding to an absorption coefficient $\alpha_M \equiv 4\pi\kappa_M/\lambda = 5\ \mu m^{-1}$ at a wavelength of 500 nm. The imaginary component of the refractive index of silicon (κ_M) strongly varies from 0.3 at 400 nm to ~0.001 at 1000 nm, while the real index of the refraction of silicon varies from 4.77 at 400 nm to 3.61 at 1000 nm [31].

Figure 1 presents the "inherent" optical interaction efficiencies calculated at the particle surface. The specific focus of the examples shown in Figs. 1(a)–1(d) is to demonstrate the changing plasmonic behavior of a 50 nm gold nanoparticle as a function of the medium absorptivity. By calculating the efficiencies

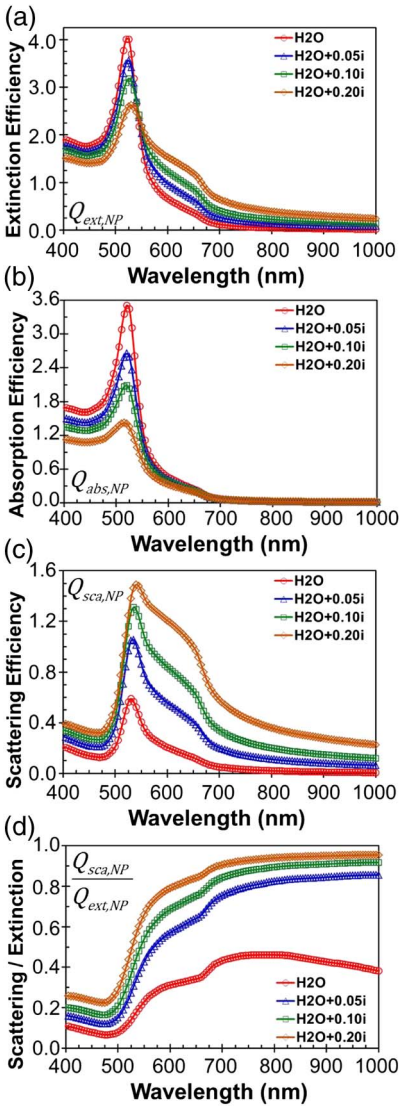

Fig. 1. Optical efficiencies of gold nanoparticles as a function of the medium absorption. The interaction efficiencies of the particle, calculated at the surface, are shown as a function of the wavelength for (a) $Q_{ext,NP}$, extinction, (b) $Q_{abs,NP}$, absorption; (c) $Q_{sca,NP}$, scattering; and (d) the fraction of scattered light in the total extinction for a 50 nm gold nanoparticle for a water-like medium with imaginary coefficients from $\kappa_M = 0 - 0.2$.

at the particle surface, we directly obtain the absorption and scattering of the particle. This method enabled us to eliminate any ambiguity [28] because of the absorption of the medium that occurs to alter the apparent values of the scattering and absorption as a function of the distance from the nanoparticle surface.

In Fig. 1(a), we see that the extinction efficiency peak of the nanosphere ($Q_{ext,NP}$) redshifts and decreases in strength as the imaginary coefficient of refraction of the medium increases. This trend also is followed by the absorption efficiency [$Q_{abs,NP}$, Fig. 1(b)], matching the findings of Quinten [32], among others. One unremarked aspect of the plasmonic response, however, is the dramatic increase in the scattering efficiency ($Q_{sca,NP}$) with an increasing imaginary component of the medium, shown in Fig. 1(c). This effect is only apparent for particles with a large imaginary part of the refractive index, such as metals, and is not observed for dielectric or weakly absorbing nanoparticles. In short, the NP plasmonic resonance redshifts, broadens, and tends toward scattering with increasing absorption in the medium.

For certain applications of plasmonic nanoparticles in absorbing media, such as in solar cells, increased scattering by the particle is an attractive goal, as it can promote enhanced absorption in the medium surrounding the nanoparticle through light trapping and provide a net gain in the near-field. Absorption by the particle, on the other hand, acts as a parasitic loss of optical intensity in this situation. We thus calculated the ratio of the scattering efficiency to the extinction efficiency ($Q_{sca,NP}/Q_{ext,NP}$), sometimes called the single-scattering albedo, which provides a scaled comparison of these terms. We found that, as the embedding medium becomes more absorbing, the absorption efficiency of the particle decreases as the scattering efficiency increases, yielding a significantly increasing scattering- to- extinction ratio [Fig. 1(d)]. This term also tends to increase with the wavelength. It can be seen that absorption is the dominant source of extinction for a 50 nm sphere in water, but that scattering is dominant for the same sphere in water with an absorbing dye at wavelengths longer than 550 nm. These results are useful in qualitatively understanding the role of absorption in the medium on the plasmonic response.

For example, we notice that even a relatively small absorption component can have a significant effect on the optical response of the particle. The nature of resonance changes because of the differences in the boundary conditions at the particle surface; the electrons at the interface are not restricted to the same degree. This phenomenon is an inherent property of the imaginary refractive index on the optical properties of the particle/environment plasmonic system. A comparison of a nanoparticle embedded in a pure dielectric medium with an equivalent magnitude refractive index does not yield the same increase in the scattering efficiency (calculations not shown here). This unremarked increase in the scattering-to-absorption ratio for nanoparticles in an absorbing medium suggests that the plasmonic enhancement of absorption by the medium could be more promising than an acquaintance with the optical properties of metal nanoparticles in a nonabsorbing medium (as they are typically synthesized, measured, and evaluated) would suggest. Increasing the particle size has a similar positive effect on the scattering-to-extinction ratio. Figure 2 shows how the extinction and scattering ratios change with increasing particle size for AuNP in water with absorbing dye [Figs. 2(a) and 2(b)] and for AuNP embedded in silicon [Figs. 2(c) and 2(d)].

The plots in Fig. 2 reveal a typical trend where the resonance peak redshifts for larger particle sizes, and splits into dipolar and quadrupolar resonances. The peak resonances are redshifted significantly with larger magnitudes for gold nanoparticles embedded in silicon on account of the increased magnitude of the index of the refraction for silicon. As expected, larger particles exhibit a more substantial scattering fraction. Here, we again have presented the "inherent" properties calculated at the sphere

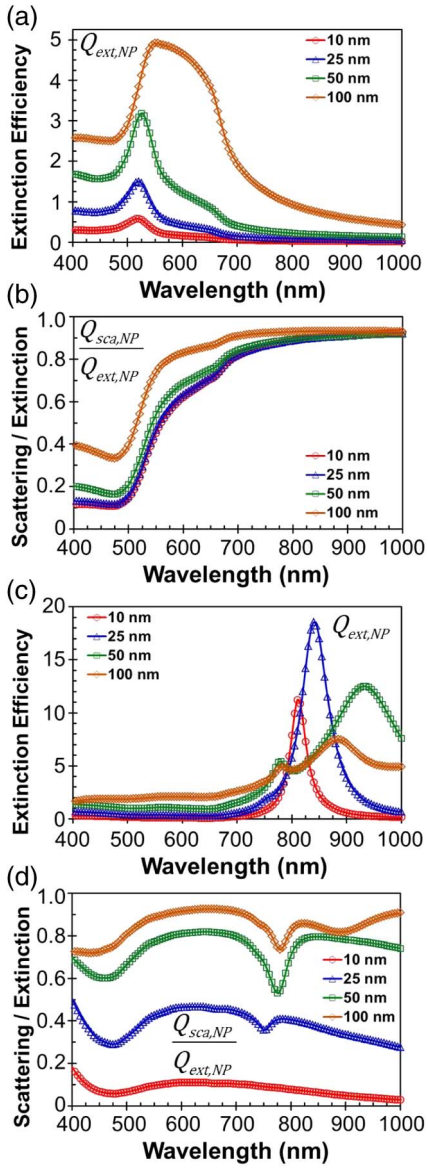

Fig. 2. Optical efficiencies of AuNP in an absorbing medium as a function of the particle size. Here, the (a) $Q_{\text{ext,NP}}$, extinction efficiency, and (b) scattered fraction of extinction are shown for AuNP in a water-like medium with $\kappa_M = 0.1$. Also shown are (c) $Q_{\text{ext,NP}}$ and (d) the scattered fraction of extinction for AuNP embedded in silicon.

surface to eliminate ambiguity that would arise from presenting far-field "apparent" interaction efficiencies.

B. Near-Field Absorption in the Medium around a Nanosphere

In this section, we calculate the amount of energy deposited in the near-field as distributed between different components, and the volume over which the energy is absorbed using our point-by-point method.

1. Near-Field Boundary Criteria

To calculate how much total energy is absorbed in the near-field (NF), we first need to determine an effective boundary for the near-field region. Here, we propose a cutoff criterion approach for quantifying the energy deposited in the near-field in absorbing media and evaluate its potential as it is applied for different electromagnetic fields enhancement values. We note that, even in the immediate vicinity to the nanoparticle, some regions will absorb more energy, while other regions will actually absorb less than would be absorbed if the particle was not present, so-called hot and cold spots, respectively [16].

Separating the near-field region from the far-field can help elucidate the different mechanisms and effects of near-field enhancement for plasmonic nanoparticles, and determine an accurate volume over which enhanced absorption occurs. A large difference can be observed between the field properties in the near-field and the far-field. In the far-field, the electric and magnetic fields can be resolved into propagating waves with a defined relationship between the magnitude and phase. In the near-field of a plasmonic particle, however, this is not the case. In addition to the propagating waves, there is also an inhomogeneous wave component that will dissipate as a function of the distance from the metal particle and will not reach the far-field. The inhomogeneous wave component exists because of the mismatch in the magnitude of the electric and magnetic fields in the near-field of a plasmonic particle in comparison with propagating light. This field can be utilized if near-field coupling can be achieved, as in near-field scanning optical microscopy, in frustrated total internal reflection, or in the presence of an absorbing medium.

An appropriate definition of the near-field would encompass the region where the majority of the added near-field absorption occurs, while also providing a contiguous region around the particle. Furthermore, the criterion should satisfy the requirement that the absorption is dominated by the incident field component outside the defined near-field region, and that this region is thus unimportant for evaluating the effect of a plasmonic nanoparticle. Within the near-field region, the energy absorbed because of each component field can be used to evaluate contributions to the total absorption of energy in the surrounding region.

The simplest boundary for separating the near- and far-field regions is a sphere of $\lambda/2\pi$ in radius, introduced in the microwave antenna field [34]. This criterion is based on the point at which the contributions of a dipole (electric field) and loop (magnetic field) elements of a hypothetical antenna become equal. While this spherical definition of boundary provides a simple rule of thumb for near-field effects, it does not provide an acceptable metric for either the shape or volume of the region of enhancement around a plasmonic nanoparticle, as the near-field region depends strongly on the material, size, and shape of the nanoparticle scatterer.

To identify the practically relevant regions of enhancement, here we define the near-field as the volume over which the local total absorption in the medium deviates from the background level. The background simply refers to the local absorption values in the absence of the nanoparticle. To identify the regions with enhanced (or reduced) optical absorption, we can therefore define the boundary as points where the absolute difference of the local near-field absorption enhancement factor, F_{AE}, from the background value exceed a small cutoff value f, satisfying $|F_{AE} - 1| > f$.

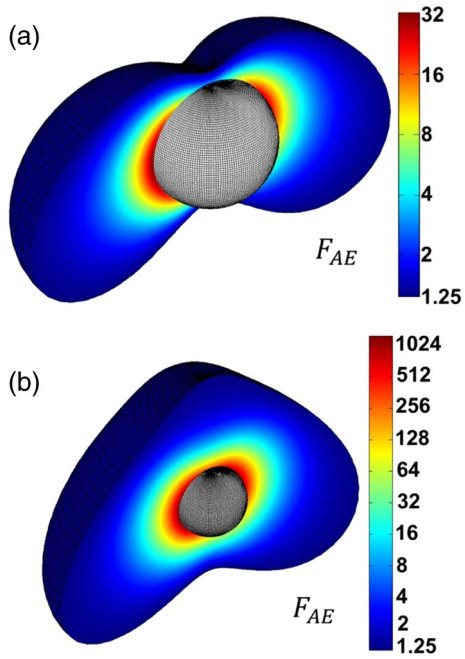

Fig. 3. Near-field volume and intensity of the near-field absorption enhancement factor, F_{AE}. The term is calculated over the region of enhanced absorption for (a) a 50 nm gold sphere in water-dye with $\kappa_M = 0.1$ on resonance at an *in vacuo* wavelength of 535 nm, and (b) a 15 nm particle embedded in silicon at 820 nm. The particle is depicted with black grid lines, and the minimum local absorption enhancement depicted is $F_{AE} = 1.25$.

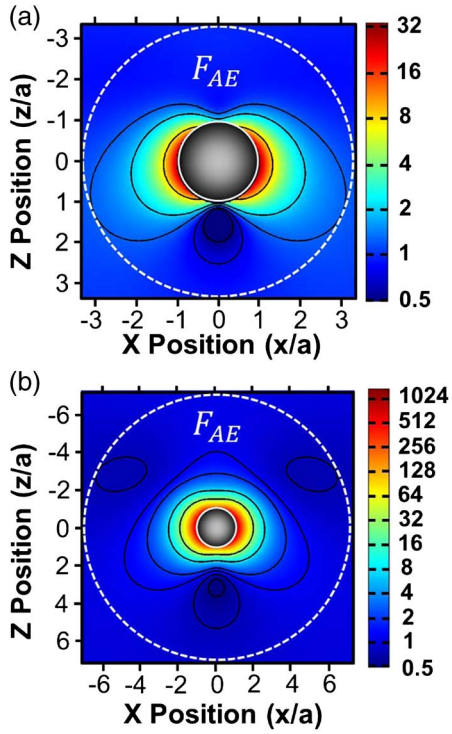

Fig. 4. Near-field absorption maps for gold nanoparticles in absorbing media. The near-field enhancement contours (solid black lines) for different enhancement values of $F_{AE} = 32$, 8, 2, and 1.25 (hot spots) and reduction values of $F_{AE} = 0.75$ and 0.5 (cold spots) in the local absorption magnitude. The maps are for (a) a 50 nm AuNP for 535 nm incident light in water with $\kappa_M = 0.1$, and (b) a 15 nm AuNP embedded in silicon. The dashed white line represents the size of a spherical volume concentric on the particle and containing the near-field enhancement contour at a cutoff value of $f = 0.25$.

A similar approach also could be taken for evaluating the extent of the near-field region in the absence of absorption, where the electromagnetic field magnitudes (electric field, magnetic field, or Poynting vector), or wave impedance (electric-to-magnetic field ratio) [35] could be used for a cutoff criterion.

The enhanced electromagnetic fields, and corresponding near-field absorption, generally decay asymptotically as a function of the distance from the particle to the background levels. Therefore, a cutoff level must be chosen to bound the near-field to regions that are experimentally relevant. As will be discussed in details below, cutoff levels of $f \geq 0.25$ provide an experimentally useful enhancement over the background for near-field absorption studies. Figure 3 presents the rapidly decaying nature of the near-field enhancement factor F_{AE} as calculated on the near-field resonance for a 50 nm gold sphere in water with an imaginary component of the refractive index $\kappa_M = 0.1$ at 535 nm, and for a 15 nm gold nanoparticle in silicon at 820 nm.

In this case, F_{AE} is much larger for the gold particle embedded in silicon because of the strong resonance and weak silicon absorption at this wavelength. It is notable that the near-field absorption enhancement is so high for the silicon case, as the particle resonance is predominantly absorbing with a scattering-to-extinction ratio is only 15% at this wavelength, showing that the near-field concentration of light can lead to high local absorption in the medium, even for a small absorbing particle. In these figures, the direction of incident wave propagation is down from the top with polarization corresponding to the direction of the enhanced regions ("lobes") shown.

Figure 4 presents the same data from Fig. 3 as a two-dimensional plot with black contours (solid black lines) added to show near-field enhancement levels. In addition to the enhanced regions with hot spots, there are regions where the absorption enhancement factor drops below the background level (cold spots), shown as the regions of 0.75 and 0.5× reduction behind the particle.

Also evident in Fig. 4 is the relatively small area occupied by the enhanced near-field region. To find the fraction of near-field absorption, we performed a point-by-point summation of the near-field absorption enhancement over all the volume elements that exceed the chosen threshold criterion, $f = 0.25$, and divided it by the absorption over the whole spherical shell volume. To find the fraction of the volume, we calculated the total volume of the near-field enhanced region, V_{NF}, through a point-by-point summation of discrete volume elements ΔV_{mno} for all points that exceed the chosen threshold criterion, and again divided it over the whole spherical volume.

The fraction of energy absorbed in the near-field within a spherical shell peaks at 67%, while the near-field region occupies less than 30% of the total volume for gold nanoparticles at

their near-field absorption resonance in a water-dye mixture, while the peak is at 96% for AuNP in silicon while occupying 54% of the volume. This peak in the absorption density occurs at a distance of 1–2 radii from the sphere surface. These results show that the majority of the near-field absorption happens very close to the particle. This phenomenon would become even more pronounced when considering nonlinear effects, where the point-by-point distribution of the enhancement field would be needed to determine photon absorption. As the distance from the sphere surface increases, the fraction of light absorbed over the near-field volume approaches the volume fraction occupied, approaching the neutral net effect level.

2. Spectral Dependence of the NF Absorption Enhancement

To further analyze the near-field properties, we also calculated the spectral dependence of the average near-field absorption enhancement, $\overline{F}_{AE}$, for several different cutoff levels (Fig. 5).

The average enhancement naturally depends on the cutoff level chosen, starting initially at a high level within a small near-field volume close to the particle and decaying monotonically as the near-field volume increases. The broad spectrum at high cutoff levels ($f = 1.0$, absorption is doubled) flattens out for cutoff levels approaching the background ($f = 0.1$). The near-field affected volume peaks at 40, 12, and 3× the particle volume for 50 nm AuNP in $H_2O + \kappa_M = 0.1$, and at 865, 70, and 26× for AuNP in Si for the cutoff $f = 1$, 0.25 and 0.1, respectively.

To understand the effect of the cutoff on the calculated near-field absorption, we calculated the enhancement of near-field absorption contributed by each component. The terms presented in Eqs. (24)–(26) can be calculated over the region exceeding a given cutoff f to provide integrated near-field values. Note that the absorption due to the incident field $Q_{\text{inc,NF}}$ occurs regardless of the presence of a nanoparticle, and is thus not shown here. Figure 6 shows the relative contribution of each field component to the near-field absorption efficiency in the immediate vicinity to the nanoparticle as a function of wavelength over the region exceeding an absolute cutoff value of $f = 0.25$. We observe that scattered light is the primary source of enhanced plasmonic absorption in the near-field. This result even holds for primarily absorbing small metal nanoparticles well off the plasmonic resonance in nearly transparent media (calculations not presented here). Interestingly, the near-field extinction efficiency can be negative at wavelengths smaller than the plasmonic peak. This interaction term provides a good indication of the perturbation of the field, which has an increasingly important contribution for larger particles at long wavelengths off-resonance. Finally, we note that the peak of the additional near-field absorption term ($Q_{\text{add,NF}}$) is redshifted from the peaks of the particle interaction efficiency terms shown in Fig. 1. This result is in agreement with Zuloaga and Nordlander, who found that the surface near-field intensity peaks at a longer wavelength than the far-field plasmonic optical interaction efficiency, indicating a deviation between near- and far-field optical properties [36].

The results presented in Figs. 5 and 6 indicate that significantly enhanced near-field absorption also can occur well off of the particle plasmon resonance and that we observe enhancement over a broad spectrum encompassing the nanoparticle plasmonic resonance. The near-field enhancement around a metal nanoparticle can be ascribed to multiple different mechanisms, such as plasmonic enhancement, the "lightning rod" effect, and field exclusion. The plasmonic effect enhances near-field electromagnetic fields as a result of the resonant oscillation of electrons drawing in light from an area much larger than the particle itself. However, we also observe near-field enhancement in the red to near-infrared region far from the plasmonic resonance for a small particle, which can be ascribed to the field exclusion effect and is indicated by the asymmetry of the resonance peak. At long wavelengths, the increased difference in the complex optical properties between the particle and the

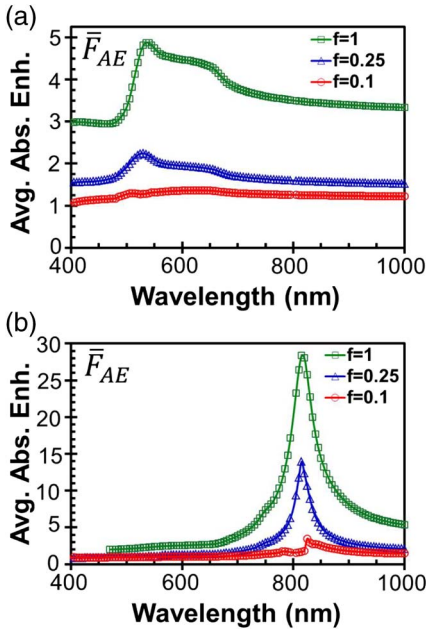

Fig. 5. Near-field average absorption enhancement $\overline{F}_{AE}$ as a function of wavelength for different cutoff criteria. The average enhancement is shown with cutoff criteria of $f = 0.1$, 0.25, and 1.0 for (a) a 50 nm gold sphere in a water medium with an imaginary refractive index coefficient $\kappa_M = 0.1$, and (b) a 15 nm gold sphere embedded in silicon.

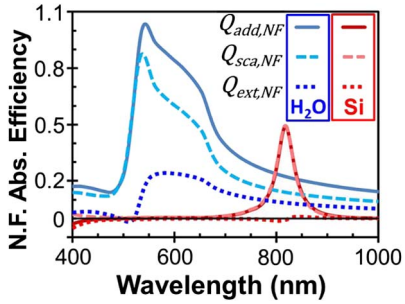

Fig. 6. Near-field absorption efficiencies ($Q_{\text{add,NF}}$, $Q_{\text{sca,NF}}$, and $Q_{\text{ext,NF}}$) for gold spheres in absorbing media. The plot shows the contributions of each field component to the near-field absorption in the medium for a fixed cutoff of $f = 0.25$ for a 50 nm AuNP in a water medium with $\kappa_M = 0.1$ (blue solid, dashed, and dotted lines), and a 15 nm AuNP embedded in Si (red solid, dashed, and dotted lines).

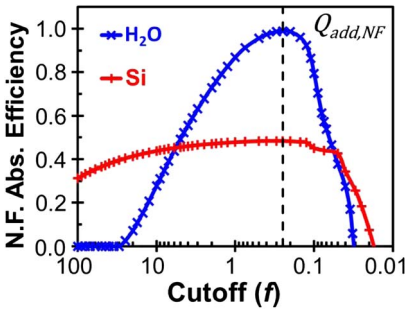

Fig. 7. Dependence of the additional local near-field absorption $Q_{\text{add,NF}}$ on the cutoff level f. $Q_{\text{add,NF}}$ is shown for a 50 nm AuNP in a water medium with $\kappa_M = 0.1$ at 535 nm (blue) and a 15 nm AuNP embedded in silicon at 820 nm (red) as a function of the cutoff f.

surroundings leads to greater rejection of the optical fields from the particle volume and enhanced electromagnetic energy densities immediately outside the particle. This leads to increased fields in the regions outside the particle volume [37].

3. Dependence of the Near-Field Absorption on the Cutoff

The effect of the cutoff on the total near-field absorption is presented in Fig. 7. The results reveal a peaked trend in the additional near-field energy deposition as the cutoff decreases and the field enhancement approaches the background level. The initial increase represents the cumulative addition of enhanced local absorption, but the total additional energy absorption eventually decays to zero as the near-field effect decays, and then eventually to the negative of the particle absorption. At low cutoff levels, detached absorption enhancement and reduction regions occur because of interference between the incident and scattered waves, and can be observed even in the case of dielectric particles. These "islands," which typically are found around five radii from the particle surface, are characterized by small deviations in the local absorption levels. Conservation of energy accounting for the energy absorbed by the particle is demonstrated by the net decrease in the absorption in the medium outside the particle.

The peak in the additional absorption is observed at $f = 0.25$ for AuNP in both water-like and silicon media, so we use this value for comparing plasmonic near-field absorption enhancement between wavelengths and particle sizes. A cutoff level of $f \geq 0.25$ also generally yields a contiguous near-field volume over a range of conditions that could provide an experimentally useful amount of enhancement over the background for near-field absorption studies.

4. Absorption of the Medium as a Function of Distance

One of the main questions we posed in the beginning of this study was to understand what dictates the near-field absorption by the medium and how scattered light contributes to this absorption. To understand the net effect and extent over which the enhanced local absorption affects, we calculated the absorption by the medium starting from the nanosphere surface to the far-field in terms of the scattered and interaction field local absorption terms, $Q_{\text{sca,NF}}$ and $Q_{\text{ext,NF}}$, and the additional near-field absorption efficiency, $Q_{\text{add,NF}}$, within a spherical radius independent of the cutoff value. In this case, the terms presented in Eqs. (24)–(26) are calculated over a concentric sphere around the nanoparticle to determine the total effect as a function of the radius. The difference between these NF values is that they include all regions over a spherical volume concentric with the particle (previously shown as the volume inside the white dotted line in Fig. 4), whereas NF values include only the near-field enhanced and decreased regions (as in the volume encompassed by the enhancement black lines in Fig. 4).

Figure 8 presents the cumulative interaction efficiencies for a spherical region around the particle as we propagate from the particle surface to the far-field. Our normalization of the near-field absorption efficiencies using the same convention as the standard plasmonic efficiencies of the nanoparticle allows us to compare the magnitudes directly. We observe that the efficiency of light absorbed by the medium from the scattered field ($Q_{\text{sca,NF}}$, blue triangles) rapidly approaches the scattering efficiency of the nanoparticle, $Q_{\text{sca,NP}}$. As expected, the scattered light is absorbed by the medium as it travels from the particle surface to the far-field. One interesting point is that much of the scattered light (~70%) is absorbed within one radius from the sphere surface (two radii, $r/a = 2$, from the center), which occurs over a wide range of absorptivities from $\kappa_M = 0.001 - 0.3$, which corresponds to the range of imaginary refractive indices for silicon from 400 to 1000 nm. The origin for the highly localized enhanced absorption close to the particle is the mismatch in the electric and magnetic fields in the plasmonic near-field. As the total scattered light proceeds out to the undisrupted far-field, the absorption approaches the level expected according to the Beer-Lambert Law of attenuation.

Figure 8 also shows the extinction efficiency of absorption by the medium from the contribution of the interaction between the incident and scattered waves ($Q_{\text{ext,NF}}$, red circles), as it converges to the negative of the extinction efficiency of the particle, $Q_{\text{ext,NP}}$. This result is an expression of the conservation of energy around a plasmonic particle. The light that is

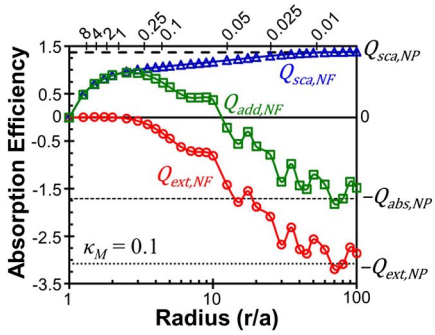

Fig. 8. Convergence of the cumulative contributing near-field terms to nanoparticle interaction efficiency values. The total absorption is shown for a 50 nm gold sphere on resonance in a water-dye medium with $\kappa_M = 0.1$ at 535 nm. Each of the field components that contribute to absorption by the medium converge to the final values related to the interaction efficiencies of the nanoparticle as the distance becomes large. This plot shows an increase in deposited energy close to the particle and the convergence to the far-field values necessitated by a conservation of energy. The marks on the top axis refer to the maximum near-field radii for the corresponding cutoff values, f.

removed by the particle from the incident light field reduces the optical energy directly available for absorption by the medium, leading to a net negative $Q_{ext,NF}$ for all radii, even though we observe a positive contribution in the near-field region. The net extra optical absorption converges to the background level of absorption only at large distances from the particle. As would be expected from a conservation of energy, near-field enhancement does not provide a net gain, but instead is an effect of a redistribution of optical energy. Thus, there is enhanced absorption near the particle for linearly absorbing media via a redistribution of absorption, but no extra absorption in total. It should be noted that this conclusion is only applicable for a quasi-infinite medium around the particle with complete absorption of the incident light. In applications where all light is not absorbed, such as thin-film optical sensors or solar cells, or where the magnitude of local absorption can have an effect, as in photodynamic therapy or in nonlinear absorption, the effect of this redistribution of light to enhance absorption near the particle could be significant.

The third curve in Fig. 8 represents the summed extra absorption in the medium because of the presence of the particle ($Q_{add,NF}$, green squares) which is the sum of the other extinction and scattering components. This curve also peaks at around two radii and shows that there are regions of net increased absorption around a plasmonic nanoparticle within a distance of around 10 radii, or $\sim\lambda$. At larger distances, around 100 radii away from the particle, this term converges to the negative of the intrinsic absorption efficiency of the nanoparticle ($Q_{abs,NP}$). This long convergence distance shows the large extent of the disruptive effect that a metal nanoparticle has on the surrounding light field for even a moderate extinction efficiency of $Q_{ext,NP} = 3.3$. However, a majority of the absorption is concentrated within a few radii away from the particle surface where a cutoff value of $f \geq 0.25$ could provide the relevant enhancement values in the near-field of the particle.

C. Particle Size and Spectral Dependence of the NF Absorption

The proposed point-by-point method can contribute greatly to large-scale parametric optimizations because of the rapidity by which calculations can be completed. To show how this method can provide useful information for such an investigation, we have studied the dependence of the near-field absorption on the particle size and spectrum for a given cutoff value. Figure 9 presents the enhanced near-field absorption for a range of gold particles sizes (5–160 nm) in the absorbing water medium [Fig. 9(a)] and silicon [Fig. 9(b)] as a function of the incoming light wavelength. The color scale in the plots represents the near-field absorption enhancement efficiency $Q_{add,NF}$. This parameter represents the extra light locally absorbed in the medium.

These plots show that the plasmonic absorption enhancement is generally low at short wavelengths far from the plasmonic response, and that the near-field absorption is positive for long wavelengths. Interestingly, a strong peak is found for small, primarily absorbing gold particles in the near-infrared in silicon, showing that the substantial field line disruption for a strongly interacting plasmonic resonance can yield significant absorption enhancement in the near-field

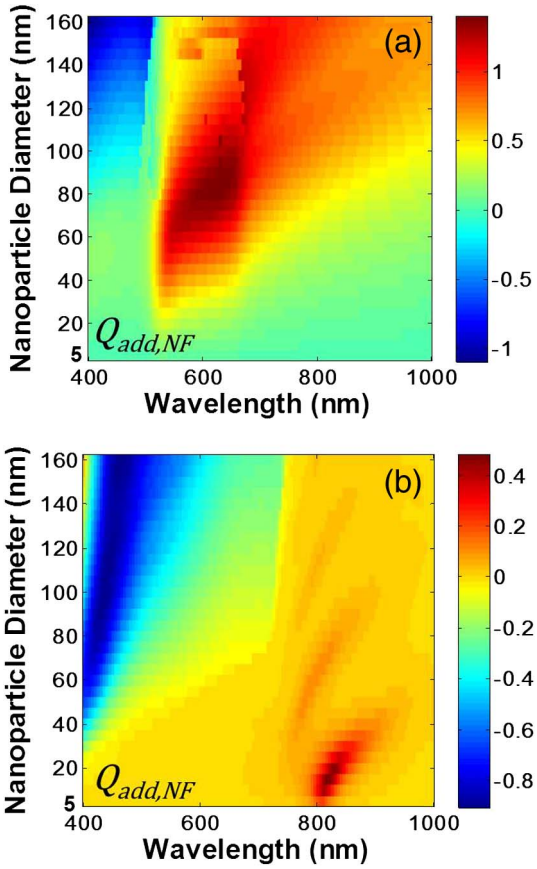

Fig. 9. Parametric study of the net local absorption enhancement as a function of the particle size and wavelength. $Q_{add,NF}$ is shown for gold nanoparticles embedded in (a) water with an added dye such that $\kappa_M = 0.1$ and (b) silicon. The cutoff value is $f = 0.25$ in these plots.

medium, as well as the particle. A full accounting of the net effect of the particles on absorption in a thin film would also need to include the angular dependent optical path length increase effect of scattering from the plasmonic particle within the absorbing media, and boundary effects such as internal scattering at interfaces and electron trapping at the surface of metal particles, as we have considered in our recent work [20]. The results here can guide us in determining the use of plasmonic particles for substantially improving the near-field absorption in a medium and the actual location of near-field enhancement necessary to define the useful maximum density of particles embedded in a medium to achieve optimal enhancement. For a thin absorbing medium in the poorly absorbed long wavelength region, where much of the light would transit the medium without absorption, this plasmonic enhancement in the near-field of the nanoparticles could have a net benefit on absorption.

5. CONCLUSIONS

In this paper, we developed analytical expressions for determining absorption in the near-field around nanospheres in absorbing media. We first showed that the ratio of scattering-to-absorption increases for plasmonic metal nanoparticles in

absorbing media. A new criterion was presented for better distinguishing the near-field region based on the calculated electromagnetic field enhancement for the near-field deposition of electromagnetic energy in absorbing media. Using this criterion, we demonstrated the calculation of near-field enhanced absorption in the near-field based on the contribution of scattered, incident, and interaction fields, showing that the scattered field was the strongest contributor to near-field enhanced absorption in the embedding medium. We found that most of the enhanced optical absorption in the medium occurs within one to two radii of the particle surface because of the extraordinary absorption of light in a region where the electromagnetic fields interact strongly, and that significant differences in absorption levels occur in close vicinity to the particle, even for primarily absorbing particles. Finally, we mapped the near-field plasmonic absorption enhancement effect in particle size and wavelength for silicon and "dyed water" media, identifying near-field absorption resonance maxima. We conclude that plasmonic enhancement can provide strong enhancement in the near-field deposition of energy in absorbing media, which will enable improved usage of near-field concentration for enhancing local absorption in the medium for technologies such as thin-film photovoltaics, optical sensing, and photochemical applications.

Funding. National Science Foundation (NSF) (Career Award CBET-0846868).

REFERENCES

1. N. J. Durr, T. Larson, D. K. Smith, B. A. Korgel, K. Sokolov, and A. Ben-Yakar, "Two-photon luminescence of cancer cells using molecularly targeted gold nanorods," Nano Lett. **7**, 941–945 (2007).
2. L. R. Hirsch, R. J. Stafford, J. A. Bankson, S. R. Sershen, B. Rivera, R. E. Price, J. D. Hazle, N. J. Halas, and J. L. West, "Nanoshell-mediated near-infrared thermal therapy of tumors under magnetic resonance guidance," Proc. Natl. Acad. Sci. USA **100**, 13549–13554 (2011).
3. D. C. Hone, P. I. Walker, R. Evans-Gowing, S. FitzGerald, A. Beeby, I. Chambrier, M. J. Cook, and D. A. Russell, "Generation of cytotoxic singlet oxygen via phthalocyanine-stabilized gold nanoparticles: a potential delivery vehicle for photodynamic therapy," Langmuir **18**, 2985–2987 (2002).
4. D. Eversole, B. Luk'yanchuk, and A. Ben-Yakar, "Plasmonic laser nanoablation of silicon by the scattering of femtosecond pulses near gold nanospheres," Appl. Phys. A **89**, 283–291 (2007).
5. R. K. Harrison and A. Ben-Yakar, "Role of near-field enhancement in plasmonic laser nanoablation using gold nanorods on a silicon substrate," Opt. Express **18**, 22556–22571 (2010).
6. P. Zijlstra, J. W. M. Chon, and M. Gu, "Five-dimensional optical recording mediated by surface plasmons in gold nanorods," Nature **459**, 410–413 (2009).
7. H. A. Atwater and A. Polman, "Plasmonics for improved photovoltaic devices," Nat. Mater. **9**, 205–213 (2010).
8. J.-J. Chen, J. C. S. Wu, P. C. Wu, and D. P. Tsai, "Plasmonic photocatalyst for H_2 evolution in photocatalytic water splitting," J. Phys. Chem. C **115**, 210–216 (2011).
9. S. Gao, K. Ueno, and H. Misawa, "Plasmonic antenna effects on photochemical reactions," Acc. Chem. Res. **44**, 251–260 (2011).
10. M. I. Stockman, "Nanoplasmonics: past, present, and glimpse into future," Opt. Express **19**, 22029–22106 (2011).
11. M. Hu and G. V. Hartland, "Heat dissipation for Au particles in aqueous solution: Relaxation time versus size," J. Phys. Chem. B **106**, 7029–7033 (2002).
12. O. Ekici, R. K. Harrison, N. J. Durr, D. S. Eversole, M. Lee, and A. Ben-Yakar, "Thermal analysis of gold nanorods heated with femtosecond laser pulses," J. Phys. D **41**, 185501 (2008).
13. A. Plech, V. Kotaidis, M. Lorenc, and J. Boneberg, "Femsosecond laser near-field ablation from gold nanoparticles," Nat. Phys. **2**, 44–47 (2005).
14. P. Leiderer, C. Bartels, J. König-Birk, M. Mosbacher, and J. Boneberg, "Imaging optical near-fields of nanostructures," Appl. Phys. Lett. **85**, 5370–5372 (2004).
15. A. Kolloch, P. Leiderer, S. Ibrahimkutty, D. Issenmann, and A. Plech, "Structural study of near-field ablation close to plasmon-resonant nanotriangles," J. Laser Appl. **24**, 042015 (2012).
16. R. A. Dynich, "Utilization efficiency of spherical metal nanoparticles that increase light absorption in absorbing media," J. Opt. Soc. Am. A **28**, 222–228 (2011).
17. J.-Y. Lee and P. Peumans, "The origin of enhanced optical absorption in solar cells with metal nanoparticles embedded in the active layer," Opt. Express **18**, 10078–10087 (2010).
18. G. Baffou, R. Quidant, and C. Girard, "Heat generation in plasmonic nanostructures," Appl. Phys. Lett. **94**, 153109 (2009).
19. R. K. Harrison and A. Ben-Yakar, "Role of near-field enhancement in plasmonic laser nanoablation using gold nanorods on a silicon substrate: reply," Opt. Express **19**, 6179–6181 (2011).
20. R. K. Harrison and A. Ben-Yakar, "Embedded Ag@SiO_2 nanoparticles for enhanced solar absorption in thin film photovoltaics," in *Proceedings of the IEEE Photonics Conference* (IEEE, 2012), pp. 58–59.
21. H. T. Miyazaki and Y. Kurokawa, "How can a resonant nanogap enhance optical fields by many orders of magnitude?" IEEE J. Sel. Topics Quantum Electron. **14**, 1565–1576 (2008).
22. A. Chimmalgi, C. P. Grigoropoulos, and K. Komvopoulos, "Surface nanostructuring by nano-/femtosecond laser-assisted scanning force microscopy," J. Appl. Phys. **97**, 104319 (2005).
23. J. D. Jackson, *Classical Electrodynamics*, 3rd ed. (Wiley, 1999).
24. G. Mie, "Beiträge zur Optik trüber Medien speziell kolloidaler Metallösungen," Ann. Phys. **330**, 377–445 (1908).
25. C. F. Bohren and D. R. Huffman, *Absorption and Scattering of Light by Small Particles* (Wiley, 2004).
26. W. C. Mundy, J. A. Roux, and A. M. Smith, "Mie scattering by spheres in an absorbing medium," J. Opt. Soc. Am. A **64**, 1593–1597 (1974).
27. I. W. Sudiarta and P. Chylek, "Mie-scattering formalism for spherical particles embedded in an absorbing medium," J. Opt. Soc. Am. A **18**, 1275–1278 (2001).
28. Q. Fu and W. Sun, "Mie theory for light scattering by a spherical particle in an absorbing medium," Appl. Opt. **40**, 1354–1361 (2001).
29. M. Daimon and A. Masamura, "Measurement of the refractive index of distilled water from the near-infrared region to the ultraviolet region," Appl. Opt. **46**, 3811–3820 (2007).
30. E. D. Palik, ed., *Handbook of Optical Constants of Solids* (Academic, 1985).
31. M. A. Green and M. J. Keevers, "Optical properties of intrinsic silicon at 300 K," Prog. Photovoltaics **3**, 189–192 (1995).
32. M. Quinten, *Optical Properties of Nanoparticle Systems* (Wiley-VCH, 2011).
33. R. A. Dynich, A. N. Ponyavina, and V. V. Filippov, "Local field enhancement near spherical nanoparticles in absorbing media," J. Appl. Spectrosc. **76**, 705–710 (2009).
34. C. Capps, "Near field or far field?" EDN Network Newsletter, 16 August 2001, pp. 95–102, http://people.eecs.ku.edu/~callen/501/Capps2001EDNpp95.pdf.
35. S. A. Schelkunoff, "The impedance concept and its application to problems of reflection, refraction, shielding and power absorption," Bell Syst. Tech. J. **17**, 17–48 (1938).
36. J. Zuloaga and P. Nordlander, "On the energy shift between near-field and far-field peak intensities in localized plasmon systems," Nano Lett. **11**, 1280–1283 (2011).
37. H. Xu, "Electromagnetic energy flow near nanoparticles-I: single spheres," J. Quant. Spectrosc. Radiat. Transfer **87**, 53–67 (2004).